LiBF$_4$ Induced Unique Surface Modification Enables Improved Electrochemical Performance of LiNi$_{0.8}$Co$_{0.1}$Mn$_{0.1}$O$_2$ Cathode

Xiaolin Zhou,[a, b] Sihan Li,[b] Ze Feng,*[b] Shan Zhang,[b] Xin Fan,*[a] Yan Wang,[b] Dan Sun,[b] Huanhuan Li,[c] Yougen Tang,[b] Haiyan Wang,*[b] Jianfeng Li,[a] and Jingchao Wei[a]

LiNi$_{0.8}$Co$_{0.1}$Mn$_{0.1}$O$_2$ (NCM811) has been regarded as a potential cathode material for next-generation lithium-ion batteries. However, the electrochemical performance of this material is severely affected by structural deterioration and capacity degradation, and the residual lithium is one of the main culprits. Herein, we propose an effective strategy to design ultrathin coatings on the surface of NCM811 by using LiBF$_4$ as the precursor. The homogeneous hybrid LiF-Li$_2$B$_4$O$_7$ coating layers can be obtained due to the reaction between LiBF$_4$ and the residual lithium, which can not only effectively reduce the

residual lithium, but also improve interfacial lithium-ion diffusion kinetics and suppress side reactions. Accordingly, the LiBF$_4$-modified samples exhibited significantly improved electrochemical performance. The coated sample of NCM811@LBF-0.7 delivers the 127.1 mAh g^{-1} discharge capacity with 69.8% capacity retention even after 300 cycles at 1 C. While the pristine sample only shows 97.1 mAh g^{-1} and the capacity retention decreases to 31.0%. This method provides a simple and effective strategy to extend the service life and safety characteristics of high-energy-density lithium-ion batteries.

Introduction

Recently, the concept of low-carbon economy has brought the electric vehicle (EV) market into a period of rapid development.[1–3] Lithium-ion batteries (LIBs) have become the main energy supply for EVs due to their advantages of high energy density, long working life, long storage period and environmental friendliness.[4–7] The thriving of EV market also stimulates the rapid development of state-of-the-art LIBs with higher energy density and low cost. It is well known that the cathode material accounts for 30%–40% of the total cost of LIBs, which is the key factor to improve the working performance of LIBs.[8] To meet the requirements of range and cost for electric vehicles, LiNi$_x$Co$_y$Mn$_{1-x-y}$O$_2$ (NCM) has been considered to be one of the most potential cathode materials for EV

batteries.[9,10] The theoretical capacity of NCM811 is about 270 mAh g^{-1}, which is much higher than other common cathode materials such as layered LiCoO$_2$ (274 mAh g^{-1}) and olivine LiFePO$_4$ (170 mAh g^{-1}) systems.[11] The reported works of literature have demonstrated that nickel is the main electroactive material, which can provide a discharge capacity of more than 200 mAh g^{-1} due to the two redox steps (Ni^{2+}↔Ni^{3+}↔Ni^{4+}) upon cycling. Cobalt can ensure the rate performance of the material, and manganese can improve the structural stability of the material.[12] Hence, Ni-rich ternary cathode (nickel content $>$60%) has aroused great interest in academia and industry. However, it has been found that the higher the content of nickel, the more serious problems for the batteries.[13]

For example, LiPF$_6$, as one of the main components of the electrolyte, is unstable and easily decomposed during the charge-discharge process.[14,15] The reaction mechanism is described as follows in Equation (1).

$$LiPF_6 \rightleftharpoons PF_5 + LiF \tag{1}$$

There is always a trace amount of H$_2$O in traditional electrolytes, which can hydrolyze PF$_5$ to form HF, as shown in Equation (2).[16] HF is aggressive to transition metals (TM) oxide and causes TM to convert into the TMF$_2$, leading to capacity loss and voltage attenuation. The specific equation is as Equation (3).[17]

$$H_2O + PF_5 \rightarrow OPF_3 + 2HF \tag{2}$$

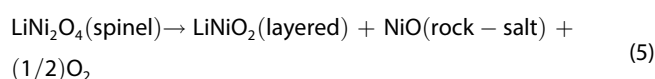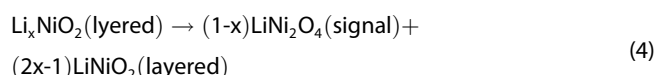$$TMO + 2HF \rightarrow TMF_2 + H_2O \tag{3}$$

[a] X. Zhou, Prof. Dr. X. Fan, J. Li, J. Wei
College of Materials Science & Engineering
Guilin University of Technology
Guilin 541004 (P. R. China)
E-mail: xfan@glut.edu.cn

[b] X. Zhou, Dr. S. Li, Dr. Z. Feng, S. Zhang, Y. Wang, Prof. Dr. D. Sun, Prof. Dr. Y. Tang, Prof. Dr. H. Wang
Shenzhen Research Institute, Hunan Provincial Key Laboratory of Chemical Power Sources
College of Chemistry and Chemical Engineering
Central South University
Changsha 410083 (P. R. China)
E-mail: fz276310095@163.com
wanghy419@csu.edu.cn

[c] Prof. Dr. H. Li
School of Chemistry and Chemical Engineering
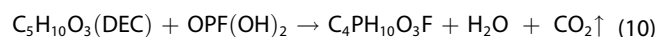Henan Normal University
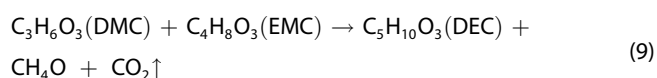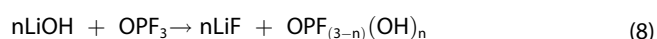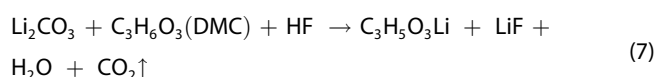Xinxiang 453007 (P. R. China)

In addition, the excess lithium (LiOH) need to be added during the preparation of NCM materials to compensate for the loss of lithium salt in the calcination process.[18] After calcination, some excess active lithium exists on the surface of the materials. After exposure, it can react with H_2O and CO_2 in the moist air to form residual lithium compounds (LiOH, $LiHCO_3$, Li_2CO_3).[19] At the same time, the valence state of Ni would spontaneously change from Ni^{3+} to Ni^{2+}, forming an inactive rock-salt phase (NiO) and resulting in the loss of lithium and oxygen. The specific equations are as follows in Equations (4) and (5).[20]

$$Li_xNiO_2(lyered) \rightarrow (1-x)LiNi_2O_4(signal) + (2x-1)LiNiO_2(layered) \tag{4}$$

$$LiNi_2O_4(spinel) \rightarrow LiNiO_2(layered) + NiO(rock-salt) + (1/2)O_2 \tag{5}$$

The micro-stress and micro-cracks of secondary particles can be formed with the phase transition, resulting in electrochemical performance degradation.[21,22]

The residual lithium on the surface of the material is similar to the insulating layer, which increases the interface impedance and affects the electrochemical performance of the battery. Moreover, the residual lithium can increase the pH value of the material, and lead to the agglomeration and gel formation of the slurry particles in the slurry preparation process.[23] Last but not the least, the residual lithium can react with the electrolyte and HF to form CO_2 gas, which also destroys the transport channel of Li^+ at the electrode interface and increase the Li^+ diffusion resistance as well as accelerate the production of lithium dendrite.[24,25] The reaction mechanisms for CO_2 generation related to residual lithium are interpreted as follows [Equations (6)–(10)]:

$$Li_2CO_3 + 2HF \rightarrow 2LiF + H_2O + CO_2\uparrow \tag{6}$$

$$Li_2CO_3 + C_3H_6O_3(DMC) + HF \rightarrow C_3H_5O_3Li + LiF + H_2O + CO_2\uparrow \tag{7}$$

$$nLiOH + OPF_3 \rightarrow nLiF + OPF_{(3-n)}(OH)_n \tag{8}$$

$$C_3H_6O_3(DMC) + C_4H_8O_3(EMC) \rightarrow C_5H_{10}O_3(DEC) + CH_4O + CO_2\uparrow \tag{9}$$

$$C_5H_{10}O_3(DEC) + OPF(OH)_2 \rightarrow C_4PH_{10}O_3F + H_2O + CO_2\uparrow \tag{10}$$
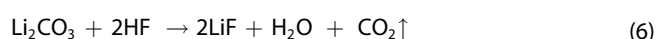
Surface coating is considered to be one of the simplest and most effective strategies to reduce the content of the residual lithium, so as to improve the structure and interface stability of the material.[26–29] Becker et al.[30] designed a simple and effective method of in situ synthesis to form a Li_2WO_4-WO_3 coating later on the surface of NCM811 material, which was derived from the reaction between ammonium tungstate and the residual lithium at high temperature, and the excess ammonium tungstate was decomposed to WO_3. The Li_2WO_4-WO_3 coating layer donated good ionic conductivity and led to improve the rate capability and cycling stability. Cheng et al.[31] coated poly(acetoacetoxyethyl methacrylate) (PAAEM) with multiple ester groups on the surface of NCM622 material, which allowed the highly reactive Ni^{4+} cation to be anchored by strong electron-donating organic groups, leading to significant improvement of cycling stability.

In this work, the homogeneous hybrid LiF-$Li_2B_4O_7$ coating layer on the surface of NCM811 has been successfully constructed by the reaction between $LiBF_4$ and the residual lithium, as depicted in Figure 1. Surface modification can effectively reduce the content of residual lithium of the cathode material. Meanwhile, the rate performance of the material is significantly improved due to the Li^+-conductors of $Li_2B_4O_7$ existence. In addition, a dense solid electrolyte membrane can be constructed because of the presence of LiF, which can prevent the erosion of the electrolyte and maintain the surface stable. As a result, the sample of NCM811@LBF-0.7 can provide 127.1 mAh g^{-1} discharge capacity after 300 cycles with 69.8% capacity retention, which is much higher than the pristine NCM811 (31.0%). Benefiting from the hybrid coating layer, the optimized NCM811 cathode exhibits such outstanding cycling performance and excellent rate capability.

Results and Discussion

Firstly, to verify the reaction between $LiBF_4$ and residual lithium compounds, a simple test was designed as follows: 2.0 g $LiBF_4$ and 2.75 g Li_2CO_3 (or 1.79 g LiOH) were mixed uniformly and heated to 500°C for 5 h in O_2 atmosphere. After grinding and crushing, the powder was characterized by XRD, and the results
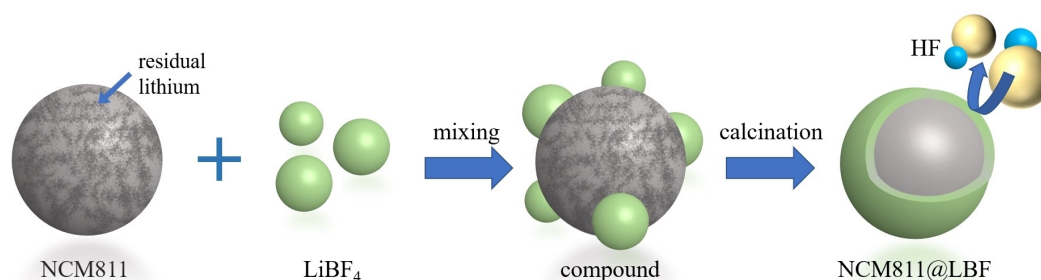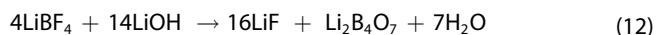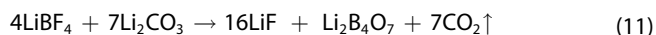

Figure 1. Schematic illustrations of a) the degradation process of NCM811 and b) the surface modification process of NCM811 by $LiBF_4$.

Batteries & Supercaps

Research Article
doi.org/10.1002/batt.202300229

Chemistry Europe
European Chemical
Societies Publishing

are shown in Figure 2(a). It is obvious that the characteristic peaks of the obtained samples are consistent with $Li_2B_4O_7$ (PDF#18-0717) and LiF (PDF#04-0857), which demonstrates that $LiBF_4$ can react with the residual lithium at 500 °C in O_2 atmosphere to form hybrid LiF-$Li_2B_4O_7$ coating layers. The reaction equations are shown as Equations (11) and (12).

$$4LiBF_4 + 7Li_2CO_3 \rightarrow 16LiF + Li_2B_4O_7 + 7CO_2\uparrow \tag{11}$$

$$4LiBF_4 + 14LiOH \rightarrow 16LiF + Li_2B_4O_7 + 7H_2O \tag{12}$$

The crystallinity structures of the pristine NCM811, NCM811@LBF-0.5, NCM811@LBF-0.7 and NCM811@LBF-1 samples were measured by X-ray diffraction (XRD). As shown in Figure 2(b), all samples exhibit clear and sharp diffraction peaks, which should be attributed to the hexagonal layered α-$NaFeO_2$ (R3 m space group) structure of NCM811 ($LiNiO_2$ PDF#09-0063).

Also, all prepared samples show clear (018)/(110) split pairs, indicating a high crystallinity and excellent layered structure.[32,33] Meanwhile, it can be seen that the original phase of the pristine NCM811 is well maintained after $LiBF_4$ coating. In addition, the peak intensity ratio of I(003)/I(104) was generally considered to be associated with the degree of mixing of the cations.[34] The values for the four samples were 1.100, 1.181, 1.357 and 1.521, which indicates that with the increase in the amount of cladding, the degree of cation mixing decreases. These experimental results suggested that the $LiBF_4$ modification does not obviously change the crystal structure or introduce an impurity phase of NCM811.

X-ray photoelectron spectroscopy (XPS) was carried out to study the surface chemical properties of pristine and modified samples (Figure 3). Figure 3(a) shows the overall survey spectra of the pristine NCM811 and NCM811@LBF-0.7 materials, and both samples exhibit a similar shape. In order to further
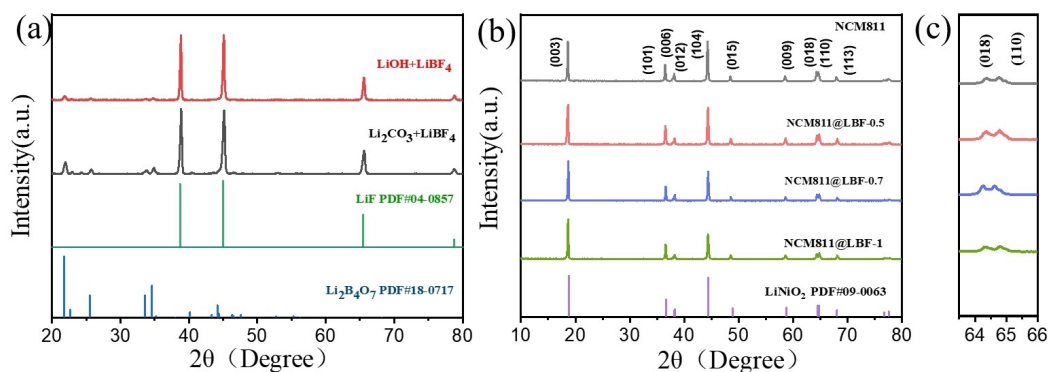

Figure 2. XRD patterns of a) the sintering products directly using $LiBF_4 + Li_2CO_3$ and $LiBF_4 + LiOH$ as raw materials, respectively; b and c) The as-prepared NCM811 samples with different content of $LiBF_4$.
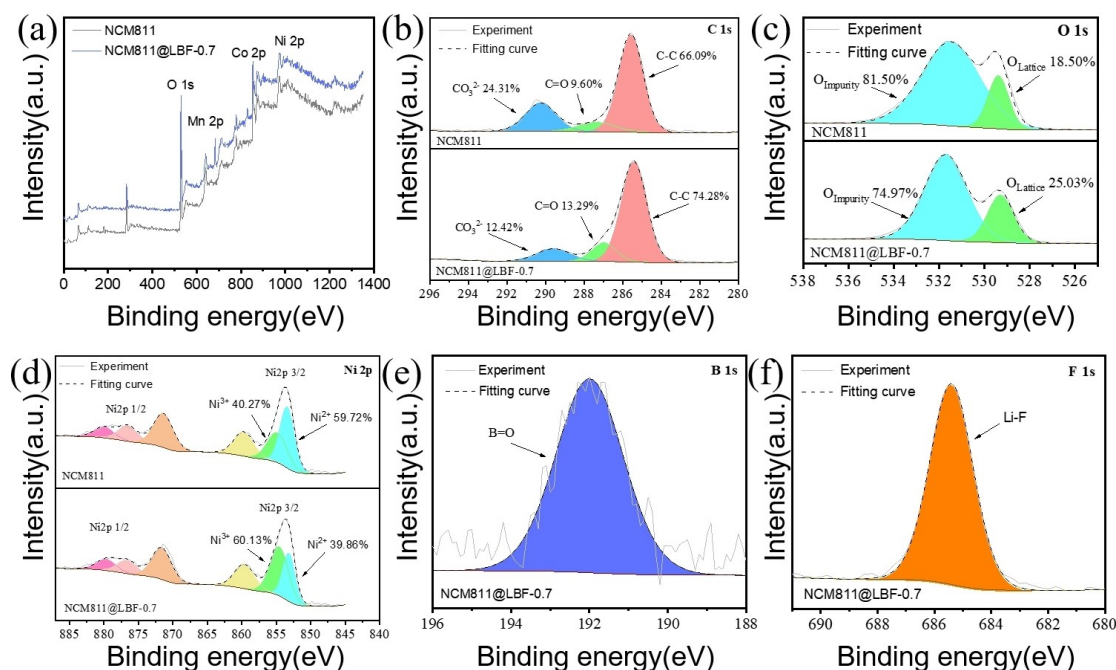

Figure 3. XPS spectra of the pristine NCM811 and NCM811@LBF-0.7 of a) survey; b) C 1s, c) O 1s, d) Ni 2p e) B 1s and f) F 1s.

investigate the changes of critical elements and chemical states of the material surface before and after modification, the C 1s, O 1s, Ni 2p, B 1s and F 1s spectra of the two samples were analyzed (Figure 3b–i). The C 1s peak of the NCM811@LBF-0.7 sample is significantly different from that of the pristine one (Figure 3b). The XPS spectrum of C 1s can be decomposed into three peaks, and the peaks at 284.9 eV and 286.4 eV can be assigned to the reference carbon (C–C and C≡O, respectively). While the other peak at 289.6 eV is assigned to residual lithium (Li_2CO_3) on the surface of the material.[35] The peak area proportion of CO_3^{2-} of the NCM811@LBF-0.7 sample (12.42%) is lower than the pristine sample (24.31%), which implies that $LiBF_4$ can effectively react with Li_2CO_3 on the surface. Figure 3(c) compares the O 1s spectra between the pristine and modified samples. The peaks of the O1s spectrum at 531.7 and 529.3 eV are assigned to $O_{impurity}$ (O^-, O^{2-}, and CO_3^{2-} of Li_2CO_3) and $O_{lattice}$ (lattice oxygen O^{2-} of M–O, M≡Ni, Co, Mn), respectively.[36] The peak area ratio of the $O_{lattice}$ in the pristine sample is 18.50%, and this value is increased to 25.03% after $LiBF_4$ involving, revealing that the structure of lattice oxygen on the surface of the material can be enhanced after coating treatment. Figure 3(d) shows the characteristic XPS spectra of Ni 2p for pristine and modified materials. The Ni^{2+} contents at the interface for NCM811 and NCM811@LBF-0.7 are 59.72% and 39.86%, while the Ni^{3+} are 40.27% and 60.13% respectively.[37] These results indicate that the interfacial modification can

effectively reduce the content of the Ni^{2+} and improve the surface stability. The peak at 192.3 eV is assigned to B≡O. Combined with the verification results in Figure 2(a), it can be concluded that the presence of $Li_2B_4O_7$ on the surface of NCM811@LBF-0.7 material.[38–40] In addition, the fluorine signal at 685.7 eV belonging to Li–F can easily be detected on the surface, suggesting the presence of LiF in the coating layer.[41,42] Based on the above analysis, we can conclude that a hybrid LiF-$Li_2B_4O_7$ coating layer has been successfully constructed on the surface of the NCM811@LBF-0.7, which can prevent corrosion of HF, inhibit the dissolution of transition metals and improve the interface stability of materials.[43,44]

Figure 4(a–d) shows the morphologies of the pristine NCM811 and NCM811@LBF-0.7. Both samples exhibit similar spherical morphology of secondary particles consisting of primary particles. However, after analyzing the high magnification images, it is found that the surface of the pristine NCM811 is relatively smooth, while many dots attached uniformly on the surface of NCM811@LBF-0.7, and those impurities should belong to the LiF-$Li_2B_4O_7$ coating layer.[36,45,46] The EDS elemental mapping analysis was used to explore the distribution of Ni, Co, Mn, O, and F elements on the surface of NCM811@LBF-0.7 (Figure 4g). It can be found that the F element is uniformly present on the surface of NCM811@LBF-0.7, but the distribution of the B element is not known due to the instrumentation.[47,48]
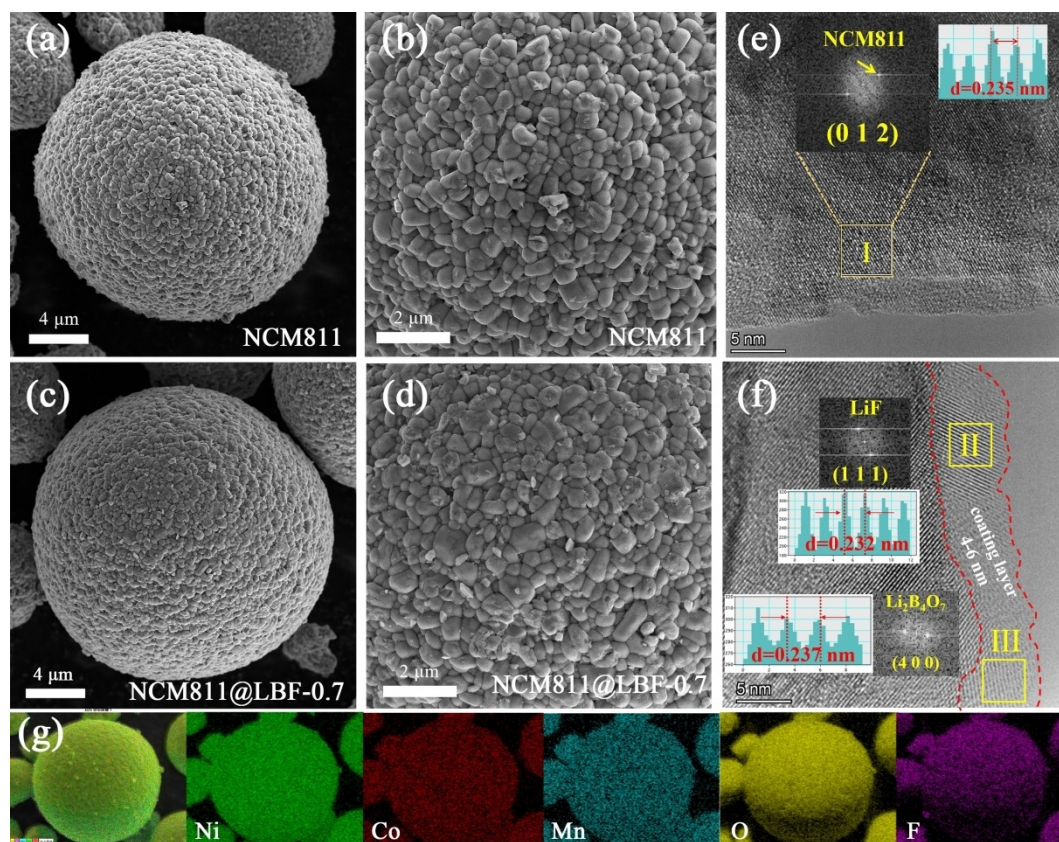

Figure 4. SEM image of a, b) the pristine NCM811 and c, d) NCM811@LBF-0.7; HR-TEM images of e) the pristine sample; f) The NCM811@LBF-0.7 sample and the corresponding FFT of the marked regions; g) The elemental mapping of NCM811@LBF-0.7

Batteries & Supercaps

Research Article
doi.org/10.1002/batt.202300229

**Chemistry
Europe**
European Chemical
Societies Publishing

Hence, in order to investigate whether there is a desirable LiF-Li$_2$B$_4$O$_7$ coating layer on the surface of the modified samples, high-resolution transmission electron microscope (HR-TEM) analysis was performed on NCM811 and NCM811@LBF-0.7, as shown in Figure 4(e and f). Clearly, the pristine NCM811 surface is smooth, with no visible adhesions on the surface, and ~0.235 nm lattice stripes can be detected in the main part (Figure 4e, part I), which is corresponding to the (012) plane of NCM811 (LiNiO$_2$, PDF#09-0063). Furthermore, a coating layer with 4–6 nm thickness is observed on the surface of the NCM811@LBF-0.7 (Figure 4f). In addition, after analyzing the HR-TEM image of the coating layer, the particular lattice fringes of (111) and (400) can be obtained with the lattice spacing of 0.232 nm (LiF, PDF#04-0857, part II) and 0.237 nm (Li$_2$B$_4$O$_7$, PDF#18-0717, part III) respectively, suggesting the existence of hybrid LiF-Li$_2$B$_4$O$_7$ coating layers.

To further confirm the change of the residual lithium change before and after coating, the pH value and the content of residual lithium of the prepared samples were analyzed by the chemical titration method. The results are shown in Table 1. It can be found that after surface modification, the pH of the

material decreases from 12.06 to 11.68 and the residual lithium content is also reduced from 1.425 wt% to 0.444 wt%. The residual lithium in the original sample should have originated from the reaction with air during the previous application, while the decrease in pH value and residual lithium content indicates that the residual lithium can be consumed during the coating process.

In order to evaluate the electrochemical performance of prepared samples, systematic electrochemical tests were carried out. Figure 5(a) shows the initial charge-discharge curves of the pristine NCM811 and NCM811@LBF-0.7 at 0.1 C between 3.0 and 4.3 V. The curve shapes of the two samples are roughly similar, indicating that the LiBF$_4$ coating does not change the basic electrochemical reaction of NCM811. At the same time, it is worth noting that the initial Coulomb efficiency of the pristine sample (84.6%) is slightly lower than the NCM811@LBF-0.7 (87.1%). Some reasons may account for this phenomenon. On one hand, the presence of the lithium impurities on the pristine hinders the direct contact between the active material and the electrolyte.[36,49] On the other hand, the coating layer consisting of Li$_2$B$_4$O$_7$ owns a positive effect on the transport of Li$^+$.[39,40,50] As can be seen from the rate capability curves in Figure 5(b), there is no significant difference between the discharge specific capacity of prepared samples at a low rate. However, the discharge capacity of the NCM811@LBF-0.7 sample at 2 C is 170.7 mAh g^{-1}, which is much higher than the original NCM811 sample (151.0 mAh g^{-1}). Compared to the pristine sample, the improved rate performance of the coated

Table 1. The pH value and the residual lithium content of NCM811 and NCM811@LBF-0.7 samples.

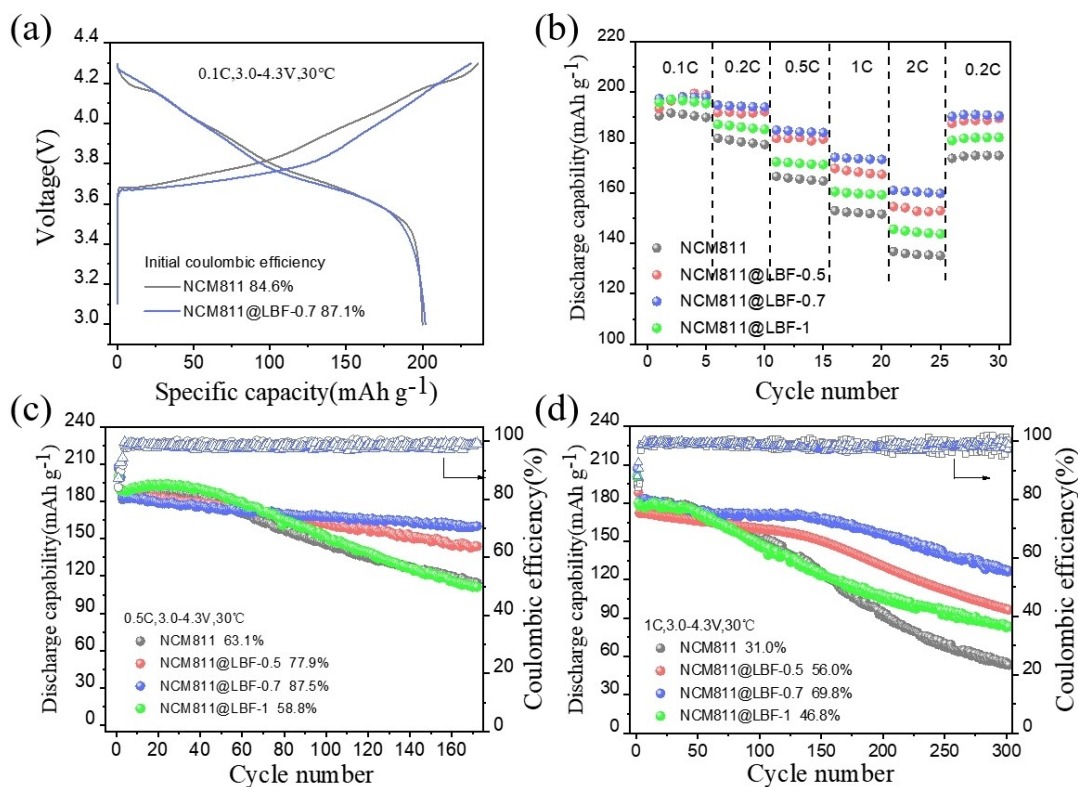| Sample	pH	Content [wt%]
NCM811	12.06	1.425
NCM811@LBF-0.7	11.68	0.444

Figure 5. a) The first charge-discharge cycle of the NCM811 and NCM811@LBF-0.7 samples between 3.0 and 4.3 V at the rate of 0.1 C; b) The rate performance of the prepared samples; c and d) The cycling performances of all samples at the rate of 0.5 C and 1 C.

sample verifies the validity of the coating treatment. In addition, The NCM811@LBF-0.7 sample also exhibits excellent cycle stability. Figure 5(c) shows the cycle curve of the prepared samples between 3.0 and 4.3 V at 0.5 C. The initial discharge specific capacities of all samples do not show a significant difference, the specific capacity of the pristine NCM811, NCM811@LBF-0.5, NCM811@LBF-0.7 and NCM811@LBF-1 samples are 114.5, 143.9, 160.2, 111.2 mAh g^{-1} after 170 cycles respectively. The NCM811@LBF-0.7 sample exhibits the best capacity retention of 87.5% in comparison with the pristine NCM811 (63.1%), NCM811@LBF-0.5 (77.9%). and NCM811@LBF-1 (58.8%). Interestingly, the NCM811@LBF-0.7 sample also provides the most excellent long cycle stability with 69.8% capacity retention even after 300 cycles at 1 C, while the

pristine NCM811, NCM811@LBF-0.5 and NCM811@LBF-1 samples only show 31.0%, 56.0% and 46.8% capacity retention respectively (Figure 5d). These results likewise suggest that an appropriate thickness of the hybrid coating layer can greatly improve the electrochemical performance of the cathode. Finally, we also compared the electrochemical data of this work with the reported references. As shown in Table 2. we can conclude that the strategy of this hybrid coating layer holds a good application potential in lithium-ion batteries.

The charge-discharge curve (Figure 6a and b) clearly shows that the coating layer also has a positive effect on the voltage attenuation problem of the battery. As shown in Figure 6(c and d), the corresponding dQ/dV curve confirm that the NCM811@LBF-0.7 sample has excellent structural properties.

Table 2. Comparison of electrochemical data of reported Ni-rich electrodes with this work.

| Material	Tested conditions	Initial discharge capacity [mAh g^{-1}]	Capacity retention	Reference
0.4 wt% Al and 0.4 wt% Zr co-doped NCM622	3–4.4 V, 30 °C	175	80.1% (100 cycles, 0.5 C)	[22]
1wt% Al(PO$_3$)$_3$ coated NCM811	3–4.3 V, 30 °C	201 (activation)	85.4% (50 cycles, 0.5 C)	[23]
3 wt% Li$_5$AlO$_4$ modified NCM811	2.8–4.3 V, 30 °C	165.57	89.15% (100 cycles, 0.5 C)	[28]
1 wt% Li$_3$PO$_4$-YPO$_4$-Y(PO$_3$)$_3$ modified degraded NCM811	3–4.3 V, 30 °C	181.01	92.3% (100 cycles, 1 C)	[36]
5 wt% Li$_2$TiO$_3$ and 5 wt% Li$_2$ZrO$_3$ co-modified NCM811	2.75–4.4 V, 25 °C	181.35	83.04% (150 cycles, 1 C)	[52]
0.7 mol% LiF-Li$_2$B$_4$O$_7$ modified NCM811	3–4.3 V, 30 °C	182.2	69.8% (300 cycles, 1 C)	This work
		183.0	87.5% (170 cycles, 0.5 C)	
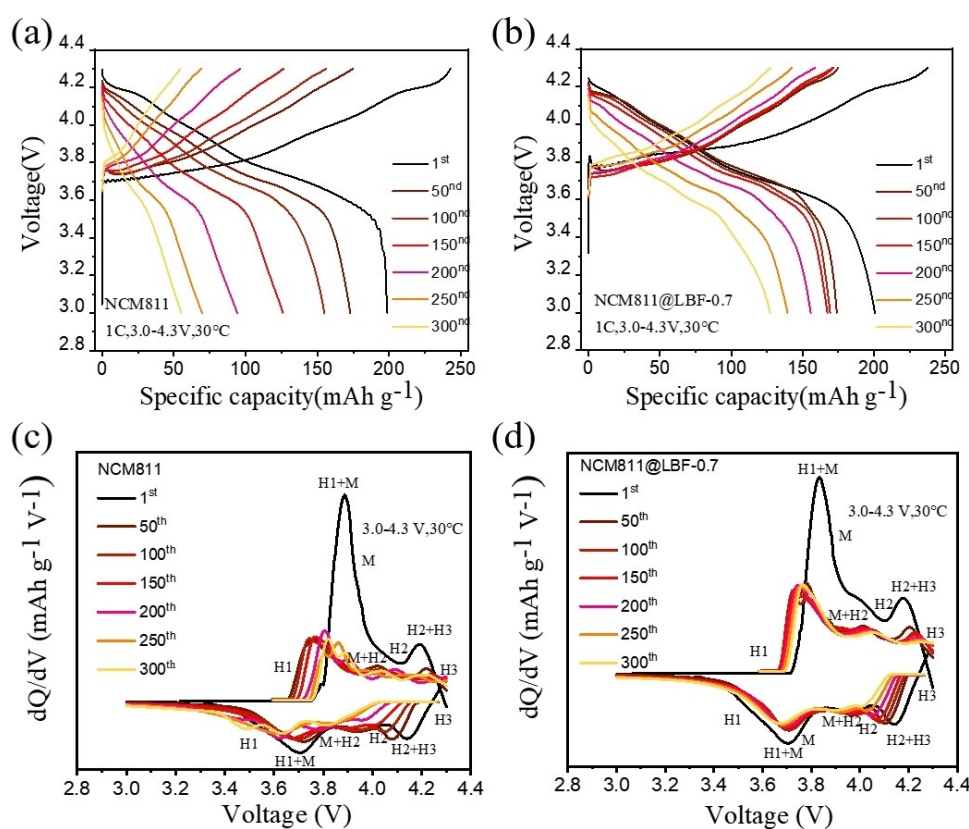
Figure 6. The charge-discharge curves of a) the pristine NCM811 and b) NCM811@LBF-0.7 at 1 C rate, c and d) are the corresponding dQ/dV profiles.
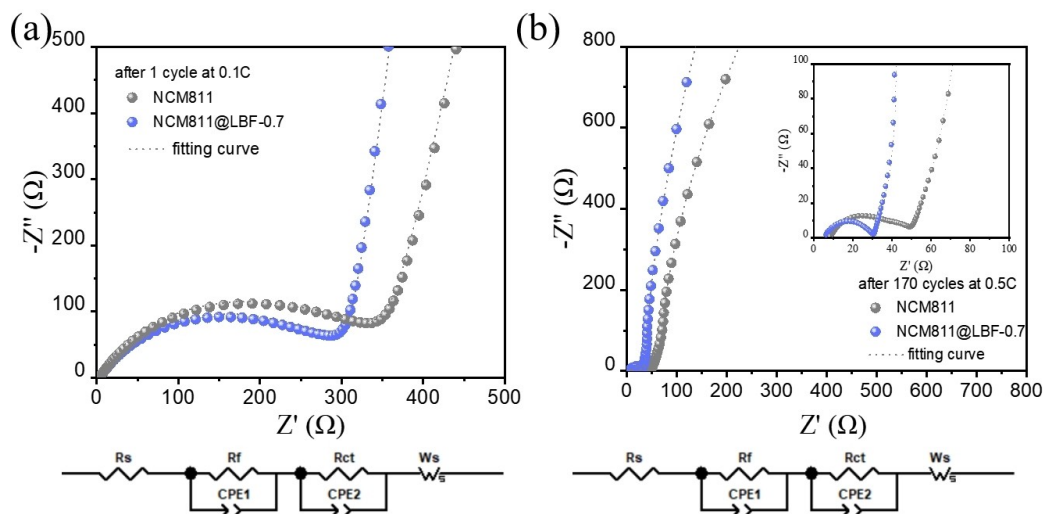
Figure 7. EIS plots of the pristine NCM811 sample and NCM811@LBF-0.7 sample after a) 1 cycle at 0.1 C and b) 170 cycles at 0.5 C.

Both samples underwent a series of phase transitions of hexagonal to monoclinic (H1→M), monoclinic to hexagonal (M→H2) and hexagonal to hexagonal (H2→H3) during charging and discharging as confirmed by three redox coupled peaks (Figure 6c and d).[51] The final H2→H3 phase transition has been demonstrated to be the key to the structural stability of materials. The peak of H2–H3 of the pristine sample almost disappears after 250 cycles, demonstrating the serious structure destruction (Figure 6c). Fortunately, the intensity of the H2→H3 peak of NCM811@LBF-0.7 is maintained well even after 300 cycles (Figure 6d), indicating that the hybrid coating layer plays a positive role in the reversibility of cycling.

To investigate the interfacial electrochemical reactions and the Li^+ kinetic behavior of the prepared samples during charge and discharge, the Nyquist diagram and equivalent circuit model of the prepared samples are shown in Figure 7. The Nyquist curve consists of two overlapping semicircles and a slope. The intercept on the Z′ axis of the Nyquist curve represents the solution resistance (R_s). The semicircles in the range of high frequency to medium frequency and low frequency can be assigned to the cathode surface facial mask (R_f) and charge transfer resistance (R_{ct}), respectively.[52] The slope line at low frequency reflects the Warburg impedance (W_s), which is related to the diffusion of lithium ions in the electrode. The fitted results are listed in Table 3. After one cycle at 0.1 C, both samples exhibit high impedance of 192.2 Ω and 123.7 Ω, which should be attributed to the forming solid electrolyte

interface (SEI) film. The impedance of both increased after cycling, which can be attributed to the SEI film formed during cycling. Moreover, the ($R_f + R_{ct}$) value of NCM811@LBF-0.7 is 207.1 Ω even after 170 cycles, which is much lower than that of the pristine sample (397.3 Ω), revealing that the hybrid coating layer is beneficial to stabilizing the interfacial Li^+ transmission channel, thereby improving the electrochemical performances for Ni-rich cathode.[53]

To study the evolution of the structure of the prepared samples during cycling, the cycled electrodes of NCM811 and NCM811@LBF-0.7 were characterized in detail by XRD. The results are shown in Figure 8(a). After long cycles of charging and discharging, the peak intensity ratio of I(003)/I(104) of the original NCM811 sample reduced from 1.100 to 0.897, while the NCM811@LBF-0.7 sample only reduced from 1.357 to 1.241. In addition, the thermal stability of nickel-rich material should be of concern because of the rapid reduction of nickel and the release of oxygen.[54] Figure 8(b) shows the DSC curves of the cathodes in the state of 4.3 V. The pristine NCM811 shows an exothermic peak at about 210.35 °C with a heat release of 918.5 J g⁻¹. In contrast, the exothermic peak of the NCM811@LBF-0.7 shifts to 217.50 °C and the heat production is reduced to 664.1 J g⁻¹. These results demonstrate that the hybrid coating layer can improve the thermal stability of the nickel-rich cathode. In order to further verify morphology change of the as-prepared samples after cycling, the particles of the pristine NCM811 and NCM811@LBF-0.7 samples after 300 cycles at 1 C were characterized by SEM. As shown in Figure 8(c and d), it is clear that many microcracks have been formed in NCM811 after 300 cycles.[55] While no obvious cracks are observed in NCM811@LBF-0.7. These results demonstrated that the LiF-Li₂B₄O₇ coating strategy can suppress the erosion of the electrolyte, improve the structural stability and reduce the crack generation.[56]

Table 3. Electrochemical impedance spectroscopy results of the pristine NCM811 and NCM811@LBF-0.7 samples.

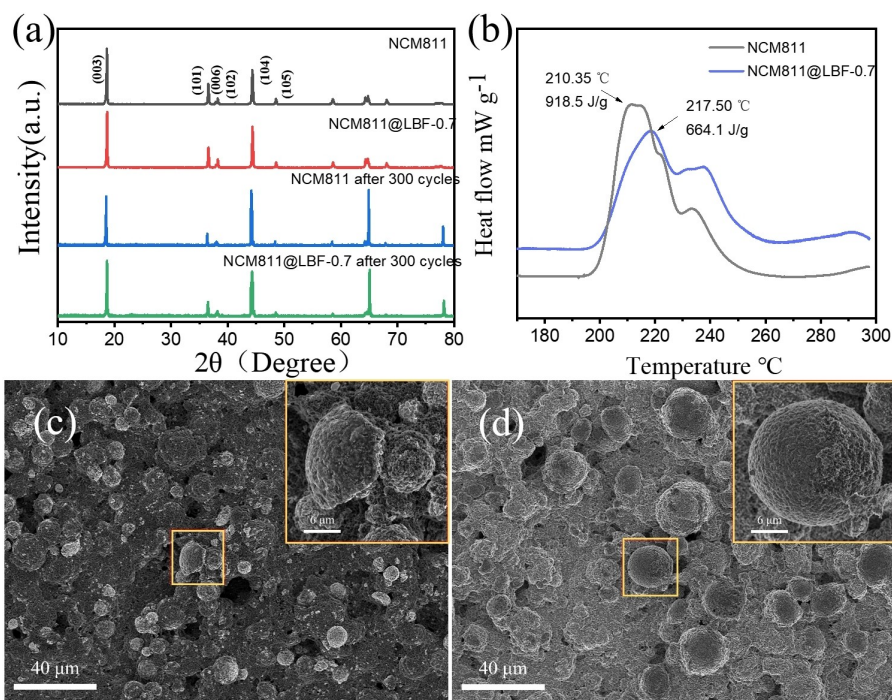|	Cycle	R_f [Ω]	R_{ct} [Ω]	$R_f + R_{ct}$ [Ω]
NCM811	1st	2.6	189.6	192.2
	170nd	76.9	320.4	397.3
NCM811@LBF-0.7	1st	3.11	120.6	123.7
	170nd	17.5	189.6	207.1

Figure 8. a) The XRD patterns of the pristine NCM811 and NCM811@LBF-0.7 electrodes before and after 300 cycles at 1 C (3.0–4.3 V); b) are the corresponding enlarged XRD view from 36° to 37°; c) The DSC profiles of NCM811 and NCM811@LBF-0.7 materials at 4.3 V charged state; SEM images of d) the pristine NCM811 and e) NCM811@LBF-0.7 sample after 300 cycles at the rate of 1 C.

Conclusions

In summary, we proposed a simple strategy to construct a uniform hybrid coating layer of LiF-$Li_2B_4O_7$ of NCM811 material and these excellent coatings derived from the reaction between $LiBF_4$ precursors and residual lithium. The generated LiF belongs to the main component of the SEI film, which is beneficial to construct a compact and stable SEI film. Meanwhile, the formed $Li_2B_4O_7$ can effectively improve the interfacial Li^+ diffusion kinetics due to their excellent ionic conductivity. Therefore, the coated sample of NCM811@LBF-0.7 shows excellent structural stability and electrochemical performance. Typically, the NCM811@LBF-0.7 exhibits 127.1 mAh g^{-1} discharge capacity with 69.8% capacity retention after 300 cycles, while the pristine sample only presents 97.1 mAh g^{-1} discharge capacity with 30.1% capacity retention. Overall, this technology by using hybrid LiF-$Li_2B_4O_7$ coating provides a new idea for the construction of nickel-rich materials with high stability, which may promote the development of high-energy-density lithium-ion batteries.

Experimental Section

Surface modification of NCM811 by lithium tetrafluoroborate

The coated samples were prepared by a wet chemical method by using commercial grade $LiNi_{0.8}Co_{0.1}Mn_{0.1}O_2$ used for 2 years at room temperature (provided by Haian Zhichuan Battery Material Technology Co., Ltd) as raw material to simulate the actual storage and transportation process. The specific preparation process was as follows: 0.0674 g $LiBF_4$ was added to ethanol and then dissolve under ultrasonic dispersion, then 10 g NCM811 cathode material was added to the solution and stirred at 90 °C until the ethanol evaporated; The powder was calcined at 500 °C for 6 h in an oxygen atmosphere. Finally, the treated materials were ground into a fine powder and passed through with a 200 mesh sieve to obtain coated NCM811. For convenience, the samples with different coating amounts of $LiBF_4$ (0 mol%, 0.5 mol%, 0.7 mol%, 1 mol%) are recorded as NCM811, NCM811@LBF-0.5, NCM811@LBF-0.7, NCM811@LBF-1, respectively.

Material characterization

The crystalline structure of the prepared samples was characterized by X-ray diffraction (XRD, Rigaku Ultima IV X-ray diffractometer) using Cu Kα radiation over the 2θ range of 10°–80° at the rate of 8° min^{-1}. The element composition and distribution of the prepared samples were determined by energy dispersive X-ray spectroscopy (EDS). The microstructure and elemental distribution of prepared samples were examined by scanning electron microscopy (SEM, Zeiss Sigma 300), and transmission electron microscopy (HR-TEM, FEI Titan G2 60-300). Surface chemical states were obtained by X-ray photoelectron spectroscopy (XPS, Thermo Fisher ESCALAB Xi+) using a multifunctional imaging electron spectrometer. The thermal stability of the charged cathodes was investigated by differential scanning calorimetry (DSC, TAQ2000).

Electrochemical measurement

The CR-2016 coin cells were assembled for electrochemical property evaluation. The cathode was prepared by slurry coating an aluminum foil. The slurry was prepared in two steps: The active material, super-P and PVDF were mixed at a mass ratio of 8:1:1, and add appropriate NMP to form homogeneous cathode

Batteries & Supercaps

Research Article
doi.org/10.1002/batt.202300229

Chemistry Europe
European Chemical
Societies Publishing

slurry. Then, the available electrode film was obtained after drying the cathode slurry at 110 °C for 12 h in the vacuum oven. Then the electrode was cut into discs with active material mass loading was about 2–3 mg and the diameter was approximately 12 mm. The electrolyte was composed of 1.0 M $LiPF_6$ dissolved in EC/DEC/EMC (1:1:1 in volume) mixture solution. The coin cells were assembled in an Ar-filled glove box with lithium metal as the anode electrode and Celgard 2400 as the separator. The charge/discharge tests were carried out on a NEWARE battery testing system (CT-4008) between 3.0 and 4.3 V (vs. Li/Li$^+$) at 30 °C (1 C = 180 mA g^{-1}) to evaluate the electrochemical properties of the prepared samples.

Acknowledgements

Conflict of Interests

There are no conflicts of interest to declare.

Data Availability Statement

Research data are not shared.

[1] Q. Luo, W. Chen, H. Fang, *Ceram. Int.* **2022**, *48*, 16737–16743.
[2] S. Luo, H. Guo, S. Feng, Z. Wang, X. Li, W. Peng, G. Yan, J. Wang, *Chem. Eng. J.* **2020**, *399*, 125142.
[3] S. Luo, H. Guo, S. Zhang, Z. Wang, X. Li, W. Peng, J. Wang, G. Yan, *J. Clean. Prod.* **2021**, *326*, 129266.
[4] J. Zhu, G. Cao, Y. Li, S. Wang, S. Deng, J. Guo, Y. Chen, T. Lei, J. Zhang, S. Chang, *Electrochim. Acta* **2019**, *325*, 134889.
[5] Z. Zhao, Y. Liu, B. Luo, J. Shen, C. Wang, J. Zhang, L. Cheng, Z. Xiao, L. Ming, B. Zhang, X. Ou, *Appl. Surf. Sci.* **2021**, *570*, 151017.
[6] D. Zuo, G. Tian, X. Li, D. Chen, K. Shu, *J. Alloys Compd.* **2017**, *706*, 24–40.
[7] U.-H. Kim, N.-Y. Park, G.-T. Park, H. Kim, C. S. Yoon, Y.-K. Sun, *Energy Storage Mater.* **2020**, *33*, 399–407.
[8] R.-M. Gao, Z.-J. Zheng, P.-F. Wang, C.-Y. Wang, H. Ye, F.-F. Cao, *Energy Storage Mater.* **2020**, *30*, 9–26.
[9] G. Shang, Y. Tang, Y. Lai, J. Wu, X. Yang, H. Li, C. Peng, J. Zheng, Z. Zhang, *J. Power Sources* **2019**, *423*, 246–254.
[10] Z. Zhao, B. Zhang, L. Cheng, Z. Liu, J. Zou, J. Zhang, B. Huang, *Mater. Lett.* **2022**, *308*, 131043.
[11] T. Tao, C. Chen, W. Qi, B. Liang, Y. Yao, S.-G. Lu, *J. Alloys Compd.* **2018**, *765*, 601–607.
[12] S. F. Amalraj, R. Raman, A. Chakraborty, N. Leifer, R. Nanda, S. Kunnikuruvan, T. Kravchuk, J. Grinblat, V. Ezersky, R. Sun, F. L. Deepak, C. Erk, X. Wu, S. Maiti, H. Sclar, G. Goobes, D. T. Major, M. Talianker, B. Markovsky, D. Aurbach, *Energy Storage Mater.* **2021**, *42*, 594–607.
[13] Y. Kim, H. Park, J. H. Warner, A. Manthiram, *ACS Energy Lett.* **2021**, *6*, 941–948.
[14] Z. Feng, X. Huang, R. Rajagopalan, Y. Tang, Z. Peng, H. Wang, *J. Electrochem. Soc.* **2019**, *166*, A1439.
[15] S. Solchenbach, M. Metzger, M. Egawa, H. Beyer, H. A. Gasteiger, *J. Electrochem. Soc.* **2018**, *165*, A3022–A3028.
[16] S. Jamil, G. Wang, M. Fasehullah, M. Xu, *J. Alloys Compd.* **2022**, *909*, 164727.
[17] S. Zhang, W. Wang, Z. Zhao, *Tribol. Int.* **2014**, *79*, 59–73.
[18] B. Chu, G. Li, L. You, T. Huang, M. Liu, A. Yu, *J. Power Sources* **2021**, *514*, 230605.
[19] Z. Feng, R. Rajagopalan, S. Zhang, D. Sun, Y. Tang, Y. Ren, H. Wang, *Adv. Sci.* **2021**, *8*, 2001809.
[20] L. Wang, T. Maxisch, G. Ceder, *Chem. Mater.* **2007**, *19*, 543–552.
[21] R. He, A. Wei, X. Bai, L. Zhang, X. Li, M. Jinping, X. Zhang, J. Ge, Z. Liu, *Ceram. Int.* **2021**, *47*, 34585–34594.
[22] Z. Feng, S. Zhang, R. Rajagopalan, X. Huang, Y. Ren, D. Sun, H. Wang, Y. Tang, *ACS Appl. Mater. Interfaces* **2021**, *13*, 43039–43050.
[23] Z. Feng, R. Rajagopalan, D. Sun, Y. Tang, H. Wang, *Chem. Eng. J.* **2020**, *382*, 122959.
[24] Z. Feng, S. Zhang, X. Huang, Y. Ren, D. Sun, Y. Tang, Q. Yan, H. Wang, *Small* **2022**, *18*, 2107346.
[25] Z. Kim, *Phys. Chem. Chem. Phys.* **2013**, *15*, 6400–6405.
[26] Z. Xiao, Z. Chi, L. Song, Z. Cao, A. Li, *Ceram. Int.* **2020**, *46*, 8328–8333.
[27] Y. Li, Z.-T. Wang, G. Liu, J. Wang, J. Wang, *Adv. Powder Technol.* **2021**, *32*, 4651–4657.
[28] J. Zhou, Q. Wang, M. Zhang, Y. Guo, A. Zhu, X. Qiu, H. Wu, X. Chen, Y. Zhang, *Electrochim. Acta* **2020**, *353*, 136541.
[29] S. H. Oh, H. J. Song, Y. Lee, J. Kim, T. Yim, *Solid State Ionics* **2021**, *370*, 115734.
[30] D. Becker, M. Börner, R. Nölle, M. Diehl, S. Klein, U. Rodehorst, R. Schmuch, M. Winter, T. Placke, *ACS Appl. Mater. Interfaces* **2019**, *11*, 18404–18414.
[31] C. Ma, M. Chen, Z. Ding, B. Wei, C. Liang, L. Zhou, L. Chen, X. Ji, P. Gao, W. Wei, *Nano Energy* **2022**, *93*, 106803.
[32] Q. Li, R. Dang, M. Chen, Y. Lee, Z. Hu, X. Xiao, *ACS Appl. Mater. Interfaces* **2018**, *10*, 17850–17860.
[33] Y. Jiang, Z. Liu, Y. Zhang, H. Hu, X. Teng, D. Wang, P. Gao, Y. Zhu, *Electrochim. Acta* **2019**, *309*, 74–85.
[34] B. Huang, D. Liu, K. Qian, L. Zhang, K. Zhou, Y. Liu, F. Kang, B. Li, *ACS Appl. Mater. Interfaces* **2019**, *11*, 14076–14084.
[35] J. Zhao, Z. Wang, J. Wang, H. Guo, X. Li, G. Yan, W. Gui, N. Chen, *Ceram. Int.* **2018**, *44*, 13341–13348.
[36] S. Zhang, Z. Feng, R. Rajagopalan, D. Sun, C. Huang, Y. Tang, Q. Yan, Y. Ren, H. Wang, *Ind. Eng. Chem. Res.* **2022**, *61*, 141–151.
[37] G. Hu, M. Zhang, L. Liang, Z. Peng, K. Du, Y. Cao, *Electrochim. Acta* **2016**, *190*, 264–275.
[38] Q. Li, W. Zhuang, Z. Li, S. Wu, N. Li, M. Gao, W. Li, J. Wang, S. Lu, *ChemElectroChem* **2020**, *7*, 998–1006.
[39] Z. Luo, G. Hu, W. Wang, K. Du, Z. Peng, J. Zeng, L. Li, Y. Cao, *J. Power Sources* **2022**, *548*, 232092.
[40] M. Li, L. Cheng, B. Zhang, P. Deng, Z. Xiao, L. Ming, Y. Zhao, B. Xu, X. Ou, *J. Alloys Compd.* **2022**, *907*, 164489.
[41] S. Pang, Y. Wang, T. Chen, X. Shen, X. Xi, D. Liao, *Ceram. Int.* **2016**, *42*, 5397–5402.
[42] K. Park, J.-H. Park, S.-G. Hong, J. Yoon, S. Park, J.-H. Kim, D. Yoon, H. Kim, Y.-H. Son, J.-H. Park, S. Kwon, *Electrochim. Acta* **2016**, *222*, 830–837.
[43] Y. Xie, D. Gao, L. L. Zhang, J. J. Chen, S. Cheng, H. F. Xiang, *Ceram. Int.* **2016**, *42*, 14587–14594.
[44] K. Yu, J. Chen, X. Xie, K. Lin, J. Li, Z. Shi, *Surf. Interfaces* **2022**, *34*, 102326.
[45] D. Wang, X. Li, Z. Wang, H. Guo, Z. Huang, L. Kong, J. Ru, *J. Alloys Compd.* **2015**, *647*, 612–619.
[46] H. Liang, Z. Wang, H. Guo, J. Wang, J. Leng, *Appl. Surf. Sci.* **2017**, *423*, 1045–1053.
[47] J. Chen, B. Su, J. Fan, B. Chu, G. Li, T. Huang, A. Yu, *Electrochim. Acta* **2022**, *422*, 140564.
[48] Y. Zhuang, Y. Zhao, Y. Bao, W. Zhang, M. Guan, *J. Alloys Compd.* **2022**, *927*, 166967.
[49] Y. Shi, G. Chen, F. Liu, X. Yue, Z. Chen, *ACS Energy Lett.* **2018**, *3*, 1683–1692.

Batteries & Supercaps

Research Article
doi.org/10.1002/batt.202300229

Chemistry Europe
European Chemical
Societies Publishing

[50] X. Cheng, J. Zheng, J. Lu, Y. Li, P. Yan, Y. Zhang, *Nano Energy* **2019**, *62*, 30–37.

[51] K. J. Park, H. G. Jung, L.-Y. Kuo, P. Kaghazchi, C. S. Yoon, Y. K. Sun, *Adv. Energy Mater.* **2018**, *8*, 1801202.

[52] J. Li, Y. Liu, W. Yao, X. Rao, S. Zhong, L. Qian, *Solid State Ionics* **2020**, *349*, 115292.

[53] Y.-G. Zou, F. Meng, D. Xiao, H. Sheng, W.-P. Chen, X.-H. Meng, Y.-H. Du, L. Gu, J.-L. Shi, Y.-G. Guo, *Nano Energy* **2021**, *87*, 106172.

[54] Y. Wang, B.-N. Liu, G. Zhou, K.-H. Nie, J.-N. Zhang, X.-Q. Yu, H. Li, *Chin. Phys. B* **2019**, *28*, 068202.

[55] T. Yim, K. S. Kang, J. Mun, S. H. Lim, S.-G. Woo, K. J. Kim, M.-S. Park, W. Cho, J. H. Song, Y.-K. Han, J.-S. Yu, Y.-J. Kim, *J. Power Sources* **2016**, *302*, 431–438.

[56] H. Li, A. Liu, N. Zhang, Y. Wang, S. Yin, H. Wu, J. R. Dahn, *Chem. Mater.* **2019**, *31*, 7574–7583.